

Prefer Nested Segmentation to Compound Segmentation

Haley D. Clark^{†,1,2}, Stefan A. Reinsberg¹, Vitali Moiseenko³,
Jon Wu^{1,4}, and Steven D. Thomas².

¹Department of Physics and Astronomy,
University of British Columbia,
6224 Agricultural Road,
Vancouver, BC, V6T 1Z1, Canada.

²Department of Medical Physics,
British Columbia Cancer Agency,
600 West Broadway,
Vancouver, BC, V5Z 4E6, Canada.

³Department of Radiation Medicine and Applied Sciences,
University of California – San Diego,
9500 Gilman Drive,
La Jolla, Ca, 92093, USA.

⁴Department of Medicine,
University of British Columbia,
2775 Laurel Street, 10th Floor,
Vancouver, BC, V5Z 1M9, Canada.

† Corresponding author: H. D. Clark, via <http://www.halclark.ca/Contact.html>.

- Disclaimer: the views expressed in this manuscript are our own and are not the official position of our employers or funders.

October 25, 2021

Abstract

Introduction: Intra-organ radiation dose sensitivity is becoming increasingly relevant in clinical radiotherapy. One method for assessment involves partitioning delineated regions of interest and comparing the relative contributions or importance to clinical outcomes. We show that an intuitive method for dividing organ contours, compound (sub-)segmentation, can unintentionally lead to sub-segments with inconsistent volumes, which will bias sub-segment relative importance assessment. An improved technique, nested segmentation, is introduced and compared.

Materials and Methods: Clinical radiotherapy planning parotid contours from 510 patients were segmented. Counts of radiotherapy dose matrix voxels interior to sub-segments were used to determine the equivalency of sub-segment volumes. The distribution of voxel counts within sub-segments were compared using Kolmogorov-Smirnov tests and characterized by their dispersion. Analytical solutions for two- and three-dimensional analogues were derived and sub-segment area/volume were compared directly.

Results: Both parotid and 2D/3D region of interest analogue segmentation confirmed compound segmentation intrinsically produces sub-segments with volumes that depend on the region of interest shape and selection location. Significant volume differences were observed when sub-segmenting parotid contours into 18^{ths}, and vanishingly small sub-segments were observed when sub-segmenting into 96^{ths}. Central sub-segments were considerably smaller than sub-segments on the periphery. Nested segmentation did not exhibit these shortcomings and produced sub-segments with equivalent volumes when dose grid and contour collinearity was addressed, even when dividing the parotid into 96^{ths}. Nested segmentation was always faster or equivalent in runtime to compound segmentation.

Conclusions: Nested segmentation is more suited than compound segmentation for analyses requiring equal weighting of sub-segments.

Keywords: Sub-segmentation; Sub-organ effects; Heterogeneous dose response; Clinical outcomes; Importance analysis.

Introduction

Heterogeneous functional dose response for organs-at-risk is becoming increasingly relevant for clinical radiotherapy planning. In 2005, [Konings et al. \(2005\)](#) found evidence of region-dependent volume effects in rat parotid. Years later in 2010, as part of the encompassing *Quantitative Analysis of Normal Tissue Effects in the Clinic* (QUANTEC) organ-focused reviews for clinical guidelines, [Deasy et al. \(2010\)](#) concluded that better predictive models were needed to model xerostomia risk. One factor recommended for investigation was whether regions within the parotid could be located that exhibited variable dose sensitivity, increased or decreased functional burden, or otherwise controlled function preservation to a higher degree than surrounding tissues. Other articles in the same report provided similar recommendations for other organs ([Rancati et al., 2010](#); [Dawson et al., 2010](#); [Pan et al., 2010](#)). In response, organ Regions of Interest (ROIs) are increasingly being segmented or handled heterogeneously to model dose response to various aspects within the organ. Reports of trials underway are emerging ([van Luijk et al., 2015](#); [Miah et al., 2016](#); [Xiao et al., 2016](#)).

Methods for complex contour segmentation, including planar segmentation, have been described in the literature ([Clark et al., 2014a](#)). A recent paper by [van Luijk et al. \(2015\)](#) made use of a planar segmentation method in which fractional volumes were used to implement a compounded Boolean sub-segment selection mechanism. Here we show that, perhaps unintuitively, such a scheme will result in sub-segments of differing volume depending on the shape of the ROI and selection location within it. Inconsistent segmentation volumes can be problematic for investigation of sub-organ effects because sub-segments will represent inconsistent portions of the whole ROI. Performing sensitivity analysis, model fitting, or tests of associativity (e.g., correlation) will result in bolstered or undermined sub-segment importance, model parameters, or associativity, which must be corrected.

We propose an improvement, which we call *nested segmentation*, that is “fair” in the sense that it will produce equal-volume sub-segments uniformly throughout the ROI when the cleaving method is free of bias. Furthermore, it is robust – if the cleaving method *is* biased, as-fair-as-possible sub-segments are produced. It is also faster than compound segmentation, requiring equivalent or less geometrical processing. An implementation based on segmentation of planar contours is tested using clinical data from 510 head-and-neck cancer patients.

We also present two methods that can be used in conjunction with segmentation that help ensure an equal number of grid voxels (e.g., radiotherapy dose matrix voxels) are contained within the boundaries of each sub-segment: oblique cleaving planes and grid supersampling. We show that both methods ameliorate issues arising from collinearity of dose grid and ROI boundaries.

Materials and Methods

Segmentation

Segmentation¹ refers to the process in which part of a volume delineated by closed contour lines (i.e., a ROI) is partitioned into connected pieces (“sub-segments”) and one or more are retained (“selected”). We refer specifically to segmentation, but the process is equivalent to *volume truncation* for polyhedra and generic *division* or *partitioning* of areas, volumes, and hypervolumes (e.g., geometric primitives, such as triangles, spheres, and cubes). Sub-segment selection can be accomplished in a variety of ways, but in this work we focus on the method described by [van Luijk et al. \(2015\)](#), which we refer to as *compound* segmentation. Our improved method, nested segmentation, is believed to be more robust toward the ‘fair distribution’ problems of ensuring that selected sub-segments have equivalent volume and contain an equivalent number of entities (e.g., dosimetric grid voxels) regardless of the ROI shape and selection location (e.g., periphery vs. centre). Salient differences are described in the following subsections.

Compound Segmentation

Compound segmentation is a planar segmentation technique that makes use of (infinite) cleaving planes. The cleaved sub-segment faces are flat, and thus when the ROI is convex all cleaved surfaces remain convex. Compound segmentation proceeds by specification of cleaving plane orientations and volume percentiles (i.e., fractional volumes). Each fractional volume ($f \in [0, 1]$) unambiguously specifies a cleaving plane which contains f on one side of the plane and $1 - f$ on the other². Each plane requires a single unit vector or two free parameters to orient the plane. In ([van Luijk et al., 2015](#)) six planes are located and used to select a sub-segment interior to the boundary of a parotid ROI. There are three sets of parallel planes; each set is orthogonal to the others (see figure 1). Use of one less plane would permit selection of an arbitrary sub-segment with a single portion of the ROI surface³, use of two less planes would permit either one or two disjoint ROI surface portions, etc..

In compound segmentation, all cleaving planes are derived using percentiles or fractional volumes that refer to the whole ROI. Only after all planes are located is segmentation performed by application of cleaving planes to the ROI volume, and only the interior is selected.

¹Alternatively *contour sub-segmentation* or just *sub-segmentation*, to differentiate it from *image* segmentation.

²Both $f = 0$ and $f = 1$ are ambiguous because they are not unique. The ambiguity is not relevant for segmentation.

³In the case of convex ROIs.

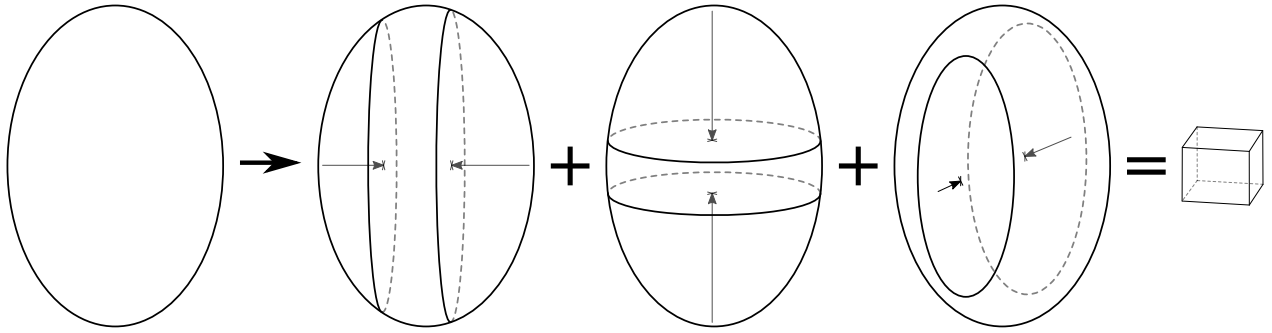


Figure 1: Demonstration of compound segmentation with three parallel pairs of mutually orthogonal planes (six planes in total).

Nested Segmentation

We propose an improved method in which sub-segments are selected as the interior region between two parallel planes, as with compound segmentation, however cleaves are performed eagerly, before the next pair of planes can be located. The location of cleaving planes are thus derived from the volume of *remaining* sub-segments, not the original ROI (see fig. 2). As each individual stage of segmentation achieves a fair divvy of the remaining volume, sub-segments are expected to always contain an equivalent portion of the ROI volume when the partitioning method is fair.

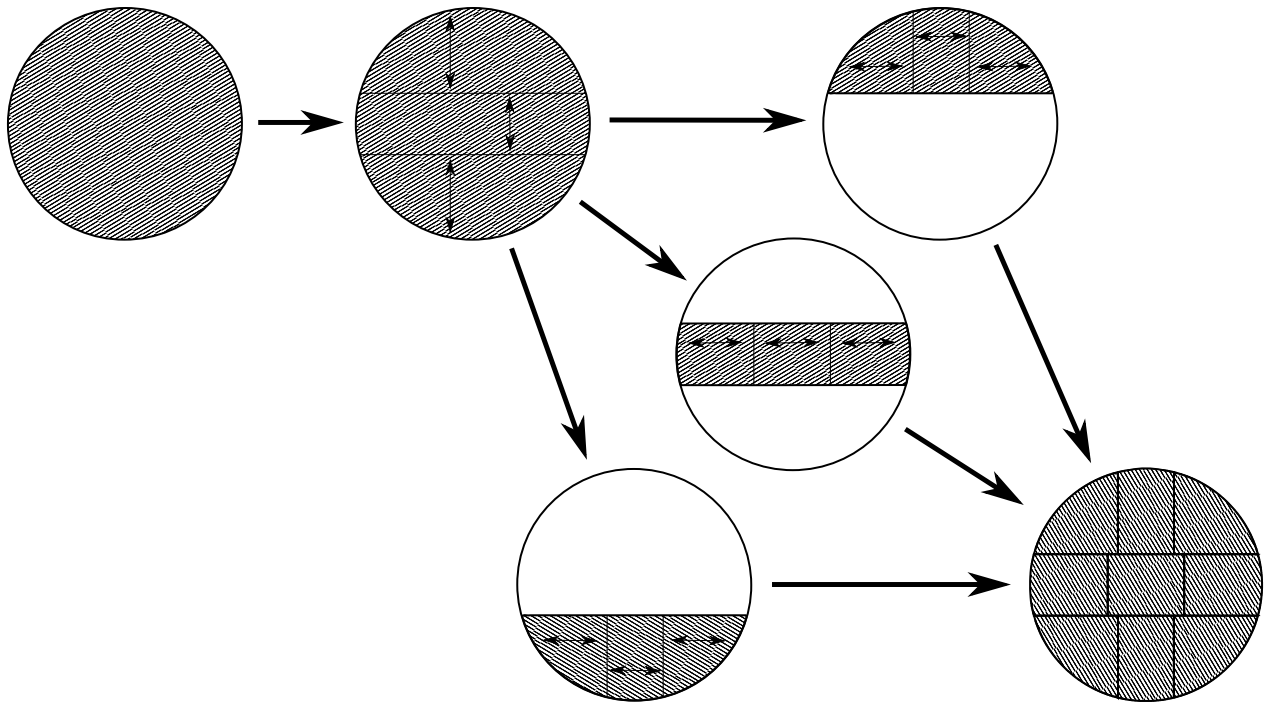


Figure 2: Demonstration of nested segmentation on a circle with $f = 1/3$. All sub-segments have area $\pi r^2/9$.

ROI Segmentation Comparison

We compare segmentation methods on a data set of 510 parotid gland ROIs from 510 head-and-neck cancer patients (one per patient, to avoid any potential bias from shape correlation between left and right parotid). We perform segmentation to generate 3, 18, and 96 sub-segments from each ROI. 18^{ths} and 96^{ths} segmentation used 6 cleaving planes (i.e., three mutually orthogonal sets of parallel planes) for each sub-segment whereas segmentation into thirds used a single pair of planes parallel to the ROI contours. Because ROIs are defined in terms of equidistant, parallel, planar contours with no gaps, contour area is used as a surrogate for volume.

Each parotid in this data set includes a radiotherapy treatment planning dosimetric grid which is used to derive dose-volume statistics of interest. We compute the number of voxels lying within each sub-segment and compare distributions for each sub-segment. Cardinal axes-aligned cleaving planes are often desired for ease of specification or bounding of anatomical regions (e.g., posterior region, lateral-caudal region, etc.). However, raster grids are commonly aligned with the cardinal directions, and are in this data set, which makes perfectly fair partitioning of voxels impossible (i.e., due to collinearity; a row locally aligned with the contour boundary is either within or outside of the sub-segment, but the row may contain many voxels). We employ two techniques which can help to more fairly partition sub-segments: raster grid supersampling and oblique cleaving planes. Supersampling used fine (15 \times) cubic interpolation so that each voxel was effectively interpolated into 225 voxels. A cyclic rotation of 22.5 $^\circ$ between cardinal axes was used to orient oblique planes.

Contours are operated on directly rather than rasterizing them onto a volumetric grid. Bisection is used to locate planes corresponding to the requisite f . The bisection method used for \mathbb{R}^3 ROI segmentation had a stopping tolerance set to 1% for all clinical data segmentation, but contours lying in planes parallel to the cleaving plane were treated atomically and were thus indivisible. Parotids with few contours therefore could not achieve 1% tolerance. Voxels for each dose matrix were of fixed volume, so summary statistics about the distribution of sub-segment voxel counts estimate sub-segment volume.

Segmentation into thirds employed only two planes parallel to contours. Nested and compound segmentation should produce identical results in this case because only a single pair of cleaves are performed. However, it is challenging because contours are not divided in this case. We include the comparison to demonstrate that bisection produces sufficiently fair sub-segments. All ROI and dose manipulations were performed using DICOM`Automaton` (Clark et al., 2014a,b).

Statistics

Distributions of volumes and voxels counts for sub-segments were compared using a non-parametric Kolmogorov-Smirnov test. The null hypothesis is that one of the distributions is drawn from

the same parent distribution as the other, so that the distributions are statistically identical. Individual sub-segment volumes are compared with other sub-segments in the same ROI using voxel counts to determine the spread due to the cumulative effects of the segmentation method and raster grid voxel alignment. The Quartile Coefficient of Dispersion (QCD) provides a normalized measure of the dispersion of sub-segment areas for each patient (Bonett, 2006). Median QCD and median-normalized ranges are reported to characterize the population. A standard statistical significance threshold (α) of 0.05 was used.

Results

Analytic Comparison

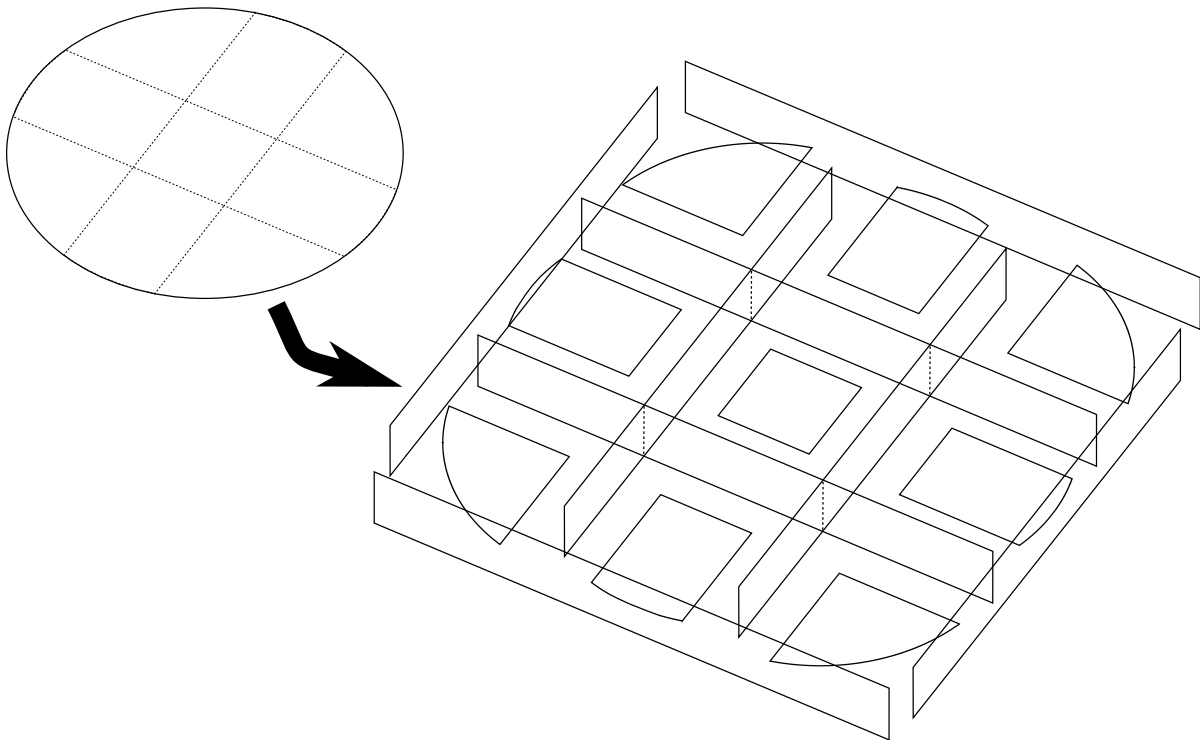


Figure 3: Partitioning of circle into nine sub-segments using compounded segmentation (exploded view). Each sub-segment is bounded by two parallel pairs of mutually orthogonal planes.

The \mathbb{R}^2 analog to ROI segmentation is individual planar contour segmentation. We segment a circle of radius r into nine sub-segments using compound segmentation (see fig. 3). The fractional area on the small side of each cleaving plane is $1/3$. Cleaving plane orientations are fixed, but the offsets from the origin are unknown and are derived analytically or located through, e.g., bisection. Using elementary methods, it can be shown that the fractional area enclosed by a plane offset

from the origin (n.b. a secant line) and a parallel plane intersecting the origin, in terms of their separation ($h \in [0, r]$; i.e., the *apothem*; cf. (Archibald, 2015)) is

$$f = \frac{2}{\pi} \left(\arcsin \frac{h}{r} + \frac{h^2}{r^2} \cot \arcsin \frac{h}{r} \right). \quad (1)$$

Inversion is used to determine h . When $f = 1/3$, $h \approx 0.264932r$. Derivation of the nine sub-segment areas is then straightforward (see fig. 4). Results are summarized in table 1. The smallest, as a ratio of the ‘fairly distributed’ area ($\pi r^2/9$) is the centre sub-segment at ≈ 0.8043 ; the centre-adjacent sub-segments are the largest at ≈ 1.0978 .

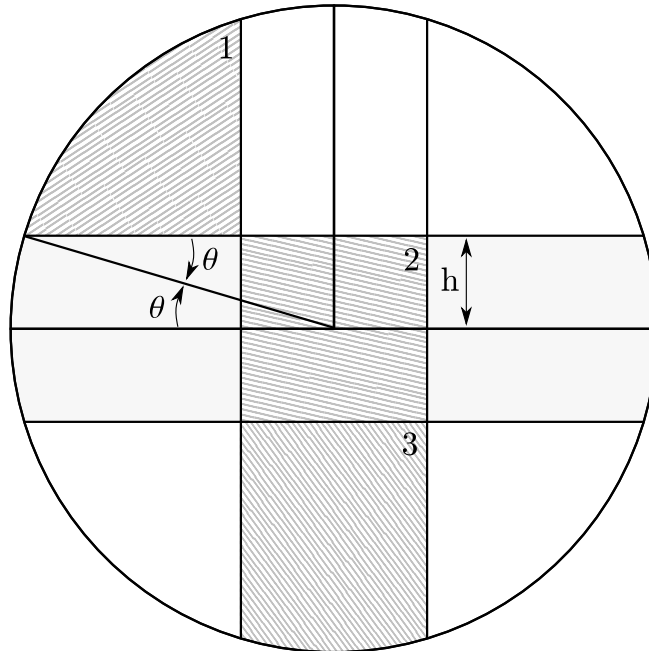


Figure 4: Calculation of sub-segment areas in terms of area of a wedge, right triangle, and square defined by $f = 1/3$, $h \approx 0.264932r$, and r . The three distinct types of sub-segments are shown: (1) “corner,” (2) “centre,” and (3) “centre-adjacent.”

Nested segmentation, on the other hand, generated sub-segments with equal area (see fig. 5). If all partitions can be made fairly, so that a cleaving plane that achieves the desired fractional areas is located exactly, then each sub-segment area is tautologically known as the product of requested fractional areas. For example, each final sub-segment in figure 2 has an area $1/3$ of $1/3$ of the total. The first cleave is identical to compound segmentation and so the apothem is given by eq. (1). Because nested segmentation is a greedy algorithm and the first cleave does not take into account later cleaves, sub-segments are in general asymmetric. The two asymmetries possible for segmentation into nine sub-segments (n.b. with fixed cleave plane orientations) are shown in fig. 5.

Sub-segment	Ratio of Fair	
	(general f)	($f = 1/3$)
centre	$\frac{36}{\pi} \left(\frac{h}{r}\right)^2$	$0.804306 \times$
centre-adjacent	$\frac{9}{2}f - \frac{18}{\pi} \left(\frac{h}{r}\right)^2$	$1.097847 \times$
corner	$\frac{9}{4}(1 - 2f) + \frac{9}{\pi} \left(\frac{h}{r}\right)^2$	$0.951077 \times$

Table 1: Ratios of the fair fractional area for compound segmentation sub-segments in terms of the apothem (h) and fractional area (f). All ratios are fractions of the fairly distributed area ($\pi r^2/9$) in which each sub-segment has an equivalent area. Centre sub-segments have four planar edges, centre-adjacent have three, and corner sub-segments have two.

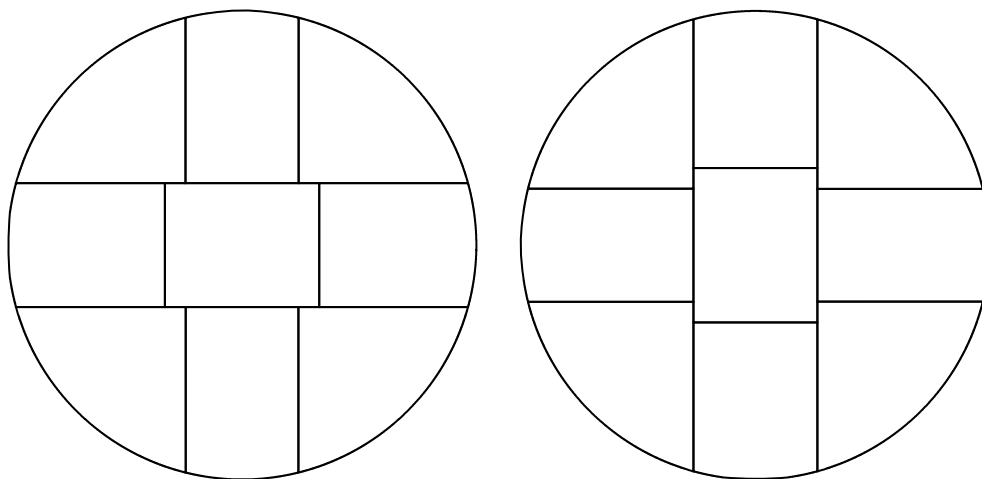


Figure 5: Nested segmentation of a circle into nine sub-segments each with area $\pi r^2/9$. The orientation of the first cleave can be chosen two ways. Both are shown. The cleaving order is important in nested segmentation but not for compound segmentation.

Moving to \mathbb{R}^3 , compound segmentation applied to a sphere partitioned into $3 \times 3 \times 3 = 27$ sub-segments yielded a centre sub-segment volume ≈ 0.596 that of the fair volume. Centre-adjacent-adjacent sub-segments had areas ≈ 1.105 that of the fair volume. Nested segmentation again produced fair volumes that were tautologically, in this case, $1/27^{\text{th}}$ of the whole. A sphere constructed of discrete stacks of contours sharing a planar orientation, which is common for medical image ROIs, approached both compound and nested segmentation results asymptotically as the contour thickness shrunk.

Segmentation into Thirds

Using compound segmentation, whole ROI were segmented into three sub-segments (f_{axial} spanned $[0, \frac{1}{3}]$, $[\frac{1}{3}, \frac{2}{3}]$, and $[\frac{2}{3}, 1]$). Bisection was employed and cleaving planes were held parallel to contours. The median number of voxels in each sub-segment spanned 587.5 – 605.0. The distribution of voxel counts in cranial, middle, and caudal sub-segments were compared with a Kolmogorov-Smirnov test. Each unique comparison in $\{\text{left, right}\}$ parotid \otimes $\{\text{cranial, middle, caudal}\}$ sub-segments was performed, yielding ten tests. In all cases the two-sided $p > 0.20$. These tests indicate the bisection approach results in appropriately partitioned sub-segments that contain 1/3 of the original parotid volume without systematic bias detectable at the $\alpha = 0.05$ level. Results were identical for nested segmentation.

Segmentation into 18^{ths}

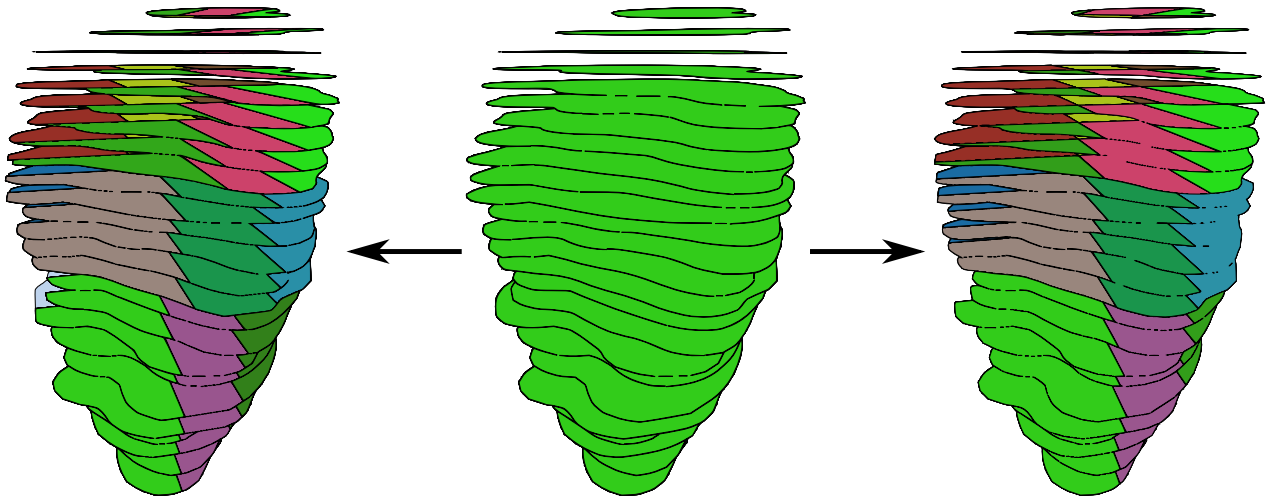


Figure 6: Depiction of nested (left) and compound (right) segmentation of whole parotid (centre) into 18 sub-segments.

Figure 6 shows nested and compound segmentation of whole parotid into 18 sub-segments. Sub-segments are composed of axially-adjacent slices coloured uniformly⁴. Both f_{axial} and f_{sagittal} spanned $[0, \frac{1}{3}]$, $[\frac{1}{3}, \frac{2}{3}]$, and $[\frac{2}{3}, 1]$; f_{coronal} spanned $[0, \frac{1}{2}]$ and $[\frac{1}{2}, 1]$. The cleaving order was axial \rightarrow coronal \rightarrow sagittal. As can be seen in figure 6, nested and compound method sub-segment locations differ only slightly. However, it is apparent that sub-segments in the compound method do not all have equivalent volume.

Using compound segmentation without supersampling or oblique cleaving planes, sub-segment voxel counts had a mean of 100.0 voxels within each sub-segment (std. dev. = 64.0; std. dev. of

⁴Colours were chosen for maximum contrast using a modification of the palette described in (Kelly, 1965).

the mean = 0.7; median = 92.0). The median number of voxels in each sub-segment spanned 38 – 152. Only 57.6% of sub-segment voxel counts had an absolute percent difference of less than 50% of the mean. Direct comparison of the voxel count distributions within sub-segments was performed using Kolmogorov-Smirnov tests. Unique comparison of all 18 sub-segments required 153 tests – in 124 cases (81%) the null hypothesis failed to be rejected and distributions were found to differ significantly (i.e., $p < 0.05$ in 124 cases). Skewness of the combined voxel count distribution was 0.991 using the ratio of moments technique, which indicates a strong positive skew. However, the mean voxel count in each *type* of sub-segment were more symmetrically distributed with a skewness of 0.075 and a std. dev. = 28.0. No significant correlation was detected between the average sub-segment mean voxel count and position relative to the parotid centre (e.g., with relativity denoted by -1 , 0 , or $+1$ in the cardinal directions).

Using nested segmentation without supersampling or oblique cleaving planes, sub-segment voxel counts again had a mean of 100.0 voxels within each sub-segment (std. dev. = 49.8; std. dev. of the mean = 0.6; median = 97.0). However the median number of voxels in each sub-segment spanned 92.5 – 101. 70.2% of sub-segment voxel counts had an absolute percent difference of less than 50% of the mean. Direct comparison of the voxel count distributions within sub-segments using Kolmogorov-Smirnov tests showed that the null hypothesis failed to be rejected in only 2 of 153 (1.3%) cases (i.e., $p < 0.05$ in 2 cases).

Segmentation into 96^{ths}

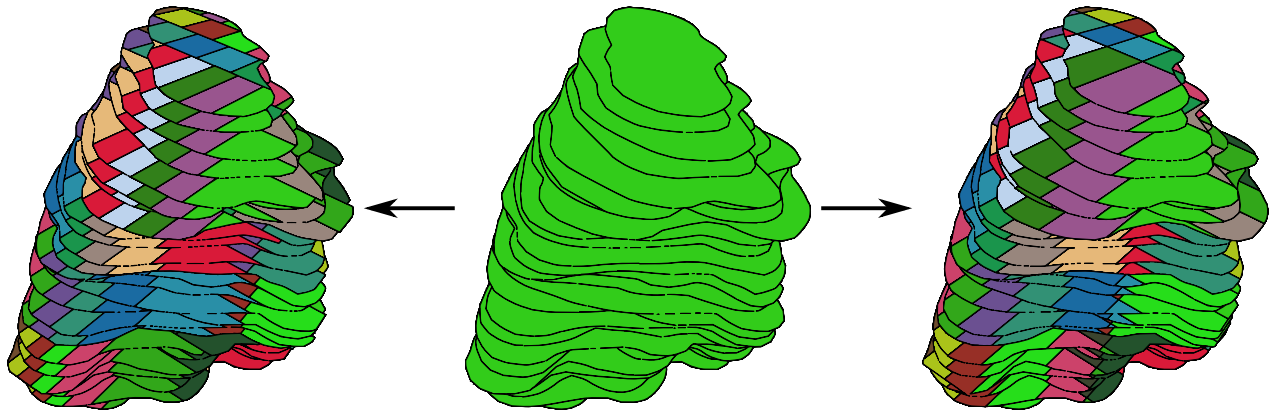


Figure 7: Depiction of nested (left) and compound (right) segmentation of whole parotid (centre) into 96 sub-segments.

For segmentation into 96^{ths}, both f_{axial} and f_{coronal} spanned $[0, \frac{1}{4}]$, $[\frac{1}{4}, \frac{1}{2}]$, $[\frac{1}{2}, \frac{3}{4}]$, and $[\frac{3}{4}, 1]$ whereas f_{sagittal} spanned $[0, \frac{1}{6}]$, $[\frac{1}{6}, \frac{1}{3}]$, $[\frac{1}{3}, \frac{1}{2}]$, $[\frac{1}{2}, \frac{2}{3}]$, $[\frac{2}{3}, \frac{5}{6}]$, and $[\frac{5}{6}, 1]$. The cleaving order was axial \rightarrow coronal \rightarrow sagittal. As can be seen in figure 7, nested and compound segmentation

again produce similar-shaped sub-segments in roughly similar locations. However, compound segmentation produces sub-segments with substantially different volumes, such as those with vanishingly small volume (in the centre-bottom of fig. 7; right side). The comparable nested segmentation sub-segments, on the other hand, are larger and have the same apparent volume as all other sub-segments (left side of fig. 7). Nested method sub-segment median QCD were less disperse than the compound method (0.097 vs. 0.37). Oblique planes reduced dispersion nearly 25 \times for nested method sub-segments (0.097 \rightarrow 0.0041). Conversely, they *increased* compound method dispersion (0.37 \rightarrow 0.46).

	Compound		Nested		
	Oblique + Supersampling	Unmodified	Oblique	Supersampling	Oblique + Supersampling
Median range	91.5 – 13829	20 – 30	18 – 20	4027.5 – 4200	4212 – 4287
Median	5558	24	19	4103	4246
Range/Median	2.47	0.417	0.105	0.042	0.018
Sig. K-S tests	2435 (53.3%)	258 (5.7%)	1 (0.02%)	0 (0%)	0 (0%)
QCD	0.46	0.097	0.0041	0.097	0.0041
Runtime	143 <i>ms</i>	36 <i>ms</i>	29 <i>ms</i>	135 <i>ms</i>	131 <i>ms</i>

Table 2: Comparison of median voxel counts, quartile coefficients of dispersion (QCD), and runtime for compound and nested segmentation. Sig. K-S tests refers to the number of statistically significant Kolmogorov-Smirnov tests (out of 4560; $\alpha = 0.05$). Runtime is per (individual) sub-segment and was measured on an Intel[®] Xeon[®] X5550 CPU. The use of oblique cleaving planes and fine supersampling reduced sub-segment median voxel range relative to the median.

A comparison of voxel counts and runtime for compound and nested segmentation is summarized in table 2. Using compound segmentation without supersampling or oblique cleaving planes led to unusable data; for each sub-segment, at least one patient had a vanishingly small sub-segment encompassing zero voxels. Using fine supersampling and oblique planes, sub-segment voxel counts had a mean of 6244.5 voxels within each sub-segment (std. dev. = 4417.6.0; std. dev. of the mean = 96.1; median = 5558.0). The median number of voxels in each sub-segment spanned 91.5 – 13829, encompassing two orders of magnitude. Direct comparison of the voxel count distributions within sub-segments via Kolmogorov-Smirnov tests showed the null hypothesis failed to be rejected and distributions were found to differ significantly in 2435 of 4560 (53.3%) unique test cases (i.e., $p < 0.05$ in 2435 cases).

Nested segmentation was markedly different. Using nested segmentation *without* supersampling or oblique planes, sub-segment voxel counts had a mean of 27.2 voxels within each sub-segment (std. dev. = 12.3; std. dev. of the mean = 0.15; median = 24.0). The median number of voxels in each sub-segment spanned 20 – 30. Direct comparison of the voxel count distributions within sub-segments via Kolmogorov-Smirnov tests showed the null hypothesis failed to be rejected and

distributions were found to differ significantly in 258 of 4560 (5.7%) unique test cases (i.e., $p < 0.05$ in 258 cases). Applying the oblique planes method yielded a mean sub-segment voxel count of 19.4 voxels within each sub-segment (std. dev. = 9.0; std. dev. of the mean = 0.04; median = 19.0). The median number of voxels in each sub-segment spanned 18 – 20. Direct comparison of the voxel count distributions within sub-segments yielded significance in a single case out of 4560 (0.02%; i.e., $p < 0.05$ for the Kolmogorov-Smirnov test in one case). Applying supersampling with axis-aligned planes yielded a mean sub-segment voxel count of 4199.3 voxels within each sub-segment (std. dev. = 2139.3; std. dev. of the mean = 9.7; median = 4103.0). The median number of voxels in each sub-segment spanned 4027.5 – 4200. No voxel count distributions were significantly distinct according to the Kolmogorov-Smirnov test (i.e., $p < 0.05$ in *zero* of 4560 tests).

Using both oblique planes and supersampling improved fairness of nested segmentation even more, though either oblique planes or supersampling alone were sufficient for most purposes. The mean sub-segment voxel count was 4270.2 voxels within each sub-segment (std. dev. = 2004.8; std. dev. of the mean = 9.1; median = 4246.0). The median number of voxels in each sub-segment spanned 4212 – 4287. Direct comparison of the voxel count distributions again found no significantly distinct distributions (i.e., $p < 0.05$ in *zero* of 4560 tests).

Discussion

Planar segmentation can be accomplished using a variety of existing tools, e.g., via Boolean structure combination (Deasy et al., 2003; Pinter et al., 2012), conversion of ROIs to polygon surface meshes and computing the intersection (The CGAL Project, 2016; Lorient et al., 2016) or via tessellation (Boots et al., 1999), or directly on ROI contours via bisection (Clark et al., 2014a). Whatever the method, sub-segments are effectively specified by the fractional volume between mutually orthogonal pairs of cleaving planes. It may then seem intuitive that sub-segments with the same fractional volume between bounding planes, but at different positions in the ROI, would have the same volume. This intuition is valid for nested segmentation, but not for compound segmentation. Compound segmentation only generates fair sub-segments when the ROI is rectangular and faces are aligned with the cleaving planes, and thus may lead to erroneous conclusions if used for sub-segment comparison. A number of articles investigating the link between patient outcomes and radiotherapy dose to parotid sub-volumes have recently emerged (Miah et al., 2016; Xiao et al., 2016; Clark et al., 2015) and use of compound segmentation has been reported in the literature (van Luijk et al., 2015). The aim of this study was to demonstrate that nested segmentation is fairer than compound segmentation, and should be preferred for analyses involving sub-segment comparison.

By analytically solving \mathbb{R}^2 and \mathbb{R}^3 analogues, we showed that compound method sub-segments have intrinsically non-uniform area/volume. In \mathbb{R}^2 , compound method centre sub-segment area

differed from that of adjacent sub-segments by nearly a *third* of the fair area. The problem grew worse in \mathbb{R}^3 with the difference assuming more than *half* the fair volume. Nested method sub-segments were fair in both cases.

The successful segmentation of clinical ROIs into thirds indicates bisection is appropriate for locating cleaving planes despite being unable to fairly partition due to discrete nature of contours along the axial direction. Compound segmentation into 18^{ths} was not fair. Distribution skewness and distinctness tests imply that the parotid was not fairly partitioned into sub-segments of equivalent volume. At the same time, the lack of correlation between sub-segment mean voxel count and relative position indicates the bisection approach is not systematically biasing results and that sub-segment volumes appear to be comparable *on average*. Nested segmentation, in comparison, was fair. Distribution distinctness test results were substantially improved compared with compound segmentation (2 vs. 124 of 153 tests found distinct distributions). The low number of distinct distributions (1.3%) was comparable with the bisection tolerance (1%) and therefore represents an acceptable deviation. Performance on the Kolmogorov-Smirnov test is notable because the transverse cleave generally can not achieve fair cleaving. The transverse cleave was performed first, and it is apparent that subsequent cleaves are fairer than those of compound segmentation.

The distinction between compound and nested segmentation was embiggened by segmentation into 96^{ths}. Some peripheral compound method sub-segments with vanishingly small volumes – even when oblique planes and intensive supersampling were employed. Nested method sub-segments were not quite fair when oblique planes and supersampling were abstained from (5.7% of Kolmogorov-Smirnov tests were significant), but this was corrected when oblique planes, supersampling, or both were employed (0.02% or less in all cases). The normalized range of voxels contained within a sub-segment dropped when using oblique planes or supersampling, indicating sub-segment volumes became fairer when either were employed. Compared to compound segmentation, nested segmentation produced normalized ranges that were two orders of magnitude smaller. Additionally, QCD differed by 1-2 orders of magnitude depending whether oblique planes were used, suggesting nested method sub-segments were substantially less disperse, and thus more uniform, than compound method sub-segments. These observation support the claim that nested segmentation is resilient to partitioning errors. When a fair cleave could not be located, i.e., due to discrete nature of contours along the axial direction, child sub-segments were made as fairly as possible (i.e., sub-segments equally shared the remaining volume with sibling sub-segments). The increase of dispersion noted in compound method sub-segments when oblique planes were used supports the claim that compound segmentation intrinsically can not fairly partition ROIs.

Nested segmentation was not only fairer than compound segmentation, but it was also faster. Sub-segments have planar edges/faces that can be described with few vertices. In nested segmentation, recursive segmentation need only process a simplified geometry for each planar edge/face. The

full ROI is processed once; afterwards, each additional segmentation is continually reduced by the increasing number of planar edges. Compound segmentation, however, must continually re-process the full ROI. The exact speed-up depends on ROI geometry, contour sampling density, and nesting depth.

One downside of nested segmentation is that the shape of sub-segments depends on the order of cleaves, resulting in shape asymmetries. A perfectly symmetrical segmentation method may be possible, but would most likely require iteration or back-tracking and re-processing whole ROIs for each sub-segment. In contrast, nested segmentation requires neither back-tracking nor re-processing geometry. Nested segmentation is directly applicable to organs where anatomical structure is ignorable or *a priori* unknown. It can also be employed within larger anatomical groupings, such as within lobes or cavities (e.g., liver, lung), and can make use of oriented cleaving planes or shuffled cleaving orders that align with local anatomy (e.g., muscle tissues, vessels, ducts). The use of planar segmentation combined with (iterated) bisection is a flexible paradigm that enables the use of individual \mathbb{R}^2 contours, raster grids, disconnected collections of contours, contours with holes, and volumetric surface manifolds, and would therefore be suitable addition to software packages that can potentially operate on any such primitives (e.g., [Pinter et al. \(2012\)](#); [Clark et al. \(2014a\)](#)).

Oblique cleaving planes addressed the issue of ROI segment and voxel grid collinearity, but can result in awkward plane orientations in some cases. There is an optimal cleave plane orientation that can be determined exactly when sub-segment extents are known⁵. This orientation maximizes the minimum spacing between voxel distances to the plane, ensuring small changes in the plane position results in the smallest possible number of voxels crossing the plane at one time (e.g., minimizing spatial resonances). Unfortunately, even estimation is difficult and costly ([Fraser, 1965](#); [Dem'yanov and Malozemov, 1974](#)) so throughout this work a cyclic rotation of 22.5° between cardinal axes defined by the Cartesian dose grid was assumed. Supersampling is also useful for improving sub-segment fairness, though it can not itself help the collinearity issue if planes are axes-aligned. However, when oblique planes and supersampling are combined, supersampling will reduce the amount of obliquity needed, which can assist in adapting to underlying anatomy. It will also result in sufficiently fair sub-segments if supersampling can be performed to an arbitrary level, though it is computationally difficult and questionable to supersample too finely. Oblique planes were more computationally efficient than supersampling, but application of either method independently for nested segmentation into 96^{ths} resulted in small median voxel ranges and acceptably indistinct distributions (i.e., $> 99.9\%$ with $p > 0.05$).

⁵The optimal angle is found for some special cases in \mathbb{R}^2 in a supplementary document.

Conclusions

Nested segmentation was found to be superior to compound segmentation when sub-segment volume consistency is needed.

Acknowledgments

This work was partially funded by a University of British Columbia Four-Year Doctoral Fellowship and by a fellowship from the Walter C. Sumner Foundation. The authors declare no conflicts of interest.

References

- Archibald, R. C. (2015). *Euclid's Book on Division of Figures: With a Restoration Based on Woepcke's Text and on the Practica Geometriae of Leonardo Pisano*. CUP Archive.
- Bonett, D. G. (2006). Confidence interval for a coefficient of quartile variation. *Computational Statistics & Data Analysis*, 50(11):2953–2957.
- Boots, B., Okabe, A., and Sugihara, K. (1999). Spatial tessellations. *Geographical information systems*, 1:503–526.
- Clark, H., Hovan, A., Moiseenko, V., Thomas, S., Wu, J., and Reinsberg, S. (2015). Regional radiation dose susceptibility within the parotid gland: Effects on salivary loss and recovery. *Medical Physics*, 42(4):2064–2071.
- Clark, H., Thomas, S., Moiseenko, V., Lee, R., Gill, B., Duzenli, C., and Wu, J. (2014a). Automated segmentation and dose-volume analysis with dicomautomaton. *Journal of Physics: Conference Series*, 489(1):012009.
- Clark, H., Wu, J., Moiseenko, V., Lee, R., Gill, B., Duzenli, C., and Thomas, S. (2014b). Semi-automated contour recognition using dicomautomaton. *Journal of Physics: Conference Series*, 489(1):012088.
- Dawson, L. A., Kavanagh, B. D., Paulino, A. C., Das, S. K., Miften, M., Li, X. A., Pan, C., Ten Haken, R. K., and Schultheiss, T. E. (2010). Radiation-associated kidney injury. *International Journal of Radiation Oncology* Biology* Physics*, 76(3):S108–S115.
- Deasy, J. O., Blanco, A. I., and Clark, V. H. (2003). Cerr: a computational environment for radiotherapy research. *Medical physics*, 30(5):979–985.
- Deasy, J. O., Moiseenko, V., Marks, L., Chao, K. C., Nam, J., and Eisbruch, A. (2010). Radiotherapy dose–volume effects on salivary gland function. *International Journal of Radiation Oncology* Biology* Physics*, 76(3):S58–S63.
- Dem‘yanov, V. F. and Malozemov, V. N. (1974). *Introduction to minimax*. Courier Corporation.
- Fraser, W. (1965). A survey of methods of computing minimax and near-minimax polynomial approximations for functions of a single independent variable. *J. ACM*, 12(3):295–314.
- Kelly, K. L. (1965). Twenty-two colors of maximum contrast. *Color Engineering*, 3(26):26–27.

- Konings, A. W., Cotteleer, F., Faber, H., van Luijk, P., Meertens, H., and Coppes, R. P. (2005). Volume effects and region-dependent radiosensitivity of the parotid gland. *International Journal of Radiation Oncology* Biology* Physics*, 62(4):1090–1095.
- Loriot, S., Tournois, J., and Yaz, I. O. (2016). Polygon mesh processing. In *CGAL User and Reference Manual*. CGAL Editorial Board, 4.9 edition.
- Miah, A., Gulliford, S., Morden, J., Newbold, K., Bhide, S., Zaidi, S., Hall, E., Harrington, K., and Nutting, C. (2016). Recovery of salivary function: Contralateral parotid-sparing intensity-modulated radiotherapy versus bilateral superficial lobe parotid-sparing intensity-modulated radiotherapy. *Clinical Oncology*.
- Pan, C. C., Kavanagh, B. D., Dawson, L. A., Li, X. A., Das, S. K., Miften, M., and Ten Haken, R. K. (2010). Radiation-associated liver injury. *International Journal of Radiation Oncology* Biology* Physics*, 76(3):S94–S100.
- Pinter, C., Lasso, A., Wang, A., Jaffray, D., and Fichtinger, G. (2012). SlicerRT: Radiation therapy research toolkit for 3d slicer. *Medical physics*, 39(10):6332–6338.
- Rancati, T., Schwarz, M., Allen, A. M., Feng, F., Popovtzer, A., Mittal, B., and Eisbruch, A. (2010). Radiation dose–volume effects in the larynx and pharynx. *International Journal of Radiation Oncology* Biology* Physics*, 76(3):S64–S69.
- The CGAL Project (2016). *CGAL User and Reference Manual*. CGAL Editorial Board, 4.9 edition.
- van Luijk, P., Pringle, S., Deasy, J. O., Moiseenko, V. V., Faber, H., Hovan, A., Baanstra, M., van der Laan, H. P., Kierkels, R. G., van der Schaaf, A., et al. (2015). Sparing the region of the salivary gland containing stem cells preserves saliva production after radiotherapy for head and neck cancer. *Science translational medicine*, 7(305):305ra147–305ra147.
- Xiao, W., Lin, Z., Zhang, W., Li, M., and Wu, V. W. (2016). A split-parotid delineation approach for dose optimization in volumetric modulated arc therapy for nasopharyngeal carcinoma patients with parapharyngeal space invasion and level IIA cervical lymph node involvements. *The British journal of radiology*, 89(1060):20150635.